LUND UNIVERSITY

Alloying and oxidation of in situ produced core-shell Al@Yb nanoalloy particles-An "on-the-fly" study.

Zhang, Chaofan; Andersson, Tomas; Mikkelä, Mikko-Heikki; Mårsell, Erik; Björneholm, Olle; Xu, Xiaojun; Tchaplyguine, Maxim; Liu, Zejin

[Link to publication](#)

Alloying and oxidation of in situ produced core-shell Al@Yb nanoalloy particles—An "on-the-fly" study

Chaofan Zhang, Tomas Andersson, Mikko-Heikki Mikkelä, Erik Mårsell, Olle Björneholm, Xiaojun Xu, Maxim Tchaplyguine, and Zejin Liu

Articles you may be interested in

Core-shell structure disclosed in self-assembled Cu-Ag nanoalloy particles
J. Chem. Phys. **138**, 104303 (2013); 10.1063/1.4794045

Optical detection of melting point depression for silver nanoparticles via in situ real time spectroscopic ellipsometry
Appl. Phys. Lett. **100**, 051107 (2012); 10.1063/1.3681367

Field dependence of the magnetocaloric effect in core-shell nanoparticles
J. Appl. Phys. **107**, 09A902 (2010); 10.1063/1.3335514

Luminescent core-shell nanostructures of silicon and silicon oxide: Nanodots and nanorods
J. Appl. Phys. **107**, 064311 (2010); 10.1063/1.3330658

Studies of thin film growth and oxidation processes for conductive Ti–Al diffusion barrier layers via in situ surface sensitive analytical techniques
Appl. Phys. Lett. **79**, 800 (2001); 10.1063/1.1391237

Alloying and oxidation of *in situ* produced core-shell Al@Yb nanoalloy particles—An "on-the-fly" study

Chaofan Zhang,[1,2] Tomas Andersson,[2] Mikko-Heikki Mikkelä,[3] Erik Mårsell,[4] Olle Björneholm,[2] Xiaojun Xu,[1] Maxim Tchaplyguine,[3,a)] and Zejin Liu[1,a)]

[1]*College of Optoelectronic Science and Engineering, National University of Defense Technology, Changsha 410073, China*
[2]*Department of Physics and Astronomy, Uppsala University, Box 516, 75120 Uppsala, Sweden*
[3]*MAX-lab, Lund University, Box 118, 22100 Lund, Sweden*
[4]*Devision of Synchrotron Radiation Research, Department of Physics, Lund University, Box 118, 22100 Lund, Sweden*

Core-shell-structured nanoalloy particles with an Al-dominated interior covered by few Yb monolayers have been fabricated using a vapor-aggregation method involving magnetron sputtering. The radially segregated structure of the Yb-Al nanoparticles has been disclosed by "on-the-fly" photoelectron spectroscopy monitoring of the nanoparticle beam in Yb 4f and Al 2p electron binding energy regions. Both, the binding energy values and the electron microscopy images taken on the deposited nanoparticles, allow estimating their dimensions to be in the 5–10 nm range. The photoelectron spectroscopy results suggest that in these nanoparticles no trivalent Yb – the typical case for the macroscopic Yb-Al alloy – is present. The oxidation of preformed Yb-Al nanoparticles was successfully attempted, leading to the appearance of divalent Yb surface oxide – in contrast to the bulk macroscopic Yb which is trivalent in the oxide. Our results suggest that at intermediate oxygen exposures "sandwich-like" nanoparticles of YbO/Yb/Al were synthesized. At higher O_2 exposures, the oxygen seems to penetrate all the way to the Yb-Al interface. The results of the present study have to be considered when photonic applications of Yb-doped garnet nanoparticles are planned. © 2014 AIP Publishing LLC. [http://dx.doi.org/10.1063/1.4893115]

I. INTRODUCTION

Multicomponent nano-structured materials containing oxides attract broad attention due to their present and perspective applications in catalysis,[1,2] solar cell technology,[3] battery design,[4] medical care,[5] photonic devices,[6–9] etc. The building blocks for these complex functional materials are in many cases nanoparticles containing one to two elements with one or both oxidized. A major attractive power of nanoparticles is the possibility to tailor their physical and chemical properties by changing their size,[10] shape,[11] atomic-scale distribution of constituent elements,[12] etc. One of the fields in which specific nanoparticle properties are already utilized is photonics. Lasers based on nanoparticle garnets – instead of the corresponding macroscopic crystals – can reach better performance.[13] Doping of nanostructured active-medium with rare earth elements, often with ytterbium, is another recent development direction in advanced laser science.[14,15] In the present work, nanoparticles consisting of elements relevant for such studies – aluminum, ytterbium, and oxygen – have been fabricated, and their electronic and geometric structure has been investigated. Being a continuation of our recent study on Yb/YbO nanoparticles,[16] the present work is at the same time a step forward in complexity of the system under the question, as it concerns *bi-metallic-nanoalloy* parti-

cles. The fabrication method is based on vapor aggregation in a cryostat,[17–19] resulting in a collimated beam of nanoparticles propagating in vacuum. Thanks to its combined element- and site-sensitivity synchrotron radiation-based photoelectron spectroscopy (PES) could be successfully employed in the present work to disclose the free nanoparticles' chemical composition and structure and that – "on the fly." Thus, the capability of the method to map the details of element distribution in multi-component nanoparticles at such demanding but – at the same time – in several ways favorable conditions has been one more time demonstrated. For most of the bi-component nanoparticles studied by us so far clear radial segregation (core-shell) structure has been observed. The stoichiometry and structure adopted by such nanoparticles have been attributed to the specificity of production kinetics and thermodynamics.[2] As in our previous works on bi-metallic nanoparticles, out of sodium and potassium,[17] and out of copper and silver,[18] the radial segregation has been explained by the difference in cohesive energy and atomic size of the two elements involved. The mobility in the formation process was high enough for the element with the lower cohesive energy to migrate to the surface of the particles.

In the present work, we first produce and characterize nanoalloy particles consisting of ytterbium and aluminum, and in the second stage we oxidize these particles using the "doping" method – similarly to our recent study on Yb oxide.[16] The result is a tri-layer radial structure with the metallic aluminum core and Yb/Yb-oxide shell.

a)Authors to whom correspondence should be addressed. Electronic addresses: maxim.tchaplyguine@maxlab.lu.se and zejinliu@vip.sina.com.

II. EXPERIMENT

As mentioned above, the nanoparticle fabrication process implemented in the present study is similar to that used in our previous work: Yb and Al vapors have been created by magnetron sputtering of a bi-component target. The sputtering target – a disc of 50 mm diameter and 6 mm thickness has been clamped out of two parts: one part of ytterbium and one of aluminum. The corresponding mono-elemental parts have been cut from commercial Yb and Al magnetron targets of 99.99% purity. The cuts have been made to get ≈40% of the total target volume out of Yb and ≈60% of Al. With this elemental ratio in the target a higher Yb vapor concentration is produced due to the higher sputtering efficiency of Yb in comparison to Al. The choice of the metal ratios has been defined by a desire to balance between different vaporization rates, ionization cross-sections for the electronic levels involved, and by specificity of the target erosion profile created by circular-magnetron sputtering.[18] Argon was employed both as sputtering and as carrier/buffer gas. The magnetron was placed inside a cryostat kept at cryogenic temperature by a continuous flow of liquid nitrogen. The metal vapor mixture aggregated in the cooled gas inside the cryostat. Approximately the same input pressure of He (as of Ar) was maintained for stabilizing the gas flow through the cryostat. A copper nozzle with a cylindrical channel of 2 mm diameter and 20 mm length was mounted at the exit of the cryostat shaping the outgoing beam. The Yb-Al nanoalloy particles formed inside the cryostat and coming out from the nozzle as a collimated particle beam were characterized by photoelectron spectroscopy. In the second stage of our investigation, the beam of Yb-Al nanoparticles created as described above was exposed to a concentric flow of oxygen. A hollow "doping" ring has 22 radial holes (of 0.6 mm diameter each) on the inner surface. The ring was mounted perpendicular to the nanoparticle beam just at the exit of the nozzle. The inner diameter of the ring is 23 mm, and its dimension along the beam is 10 mm. The oxygen pressure inside the doping ring could be regulated in a fine way by a high precision dozing valve and controlled by a gas-independent gauge. As mentioned above, the oxidation-by-doping procedure has previously been proved to work in our studies on YbO/Yb nanoparticles[16] and on Al oxide nanoparticles.

Downstream the doping ring, at the entrance to the ionization chamber, a conical skimmer with a 2-mm orifice has been placed. The skimmer cut away the larger part of argon and helium, thus reducing the gas flow from the nanoparticle source to the ionization chamber. The nanoparticle source was attached to the ionization chamber via a CF 150 port. The pressure in the nanoparticle source during the operation was in the 10^{-4}–10^{-3} mbar range, while lower than 10^{-5} mbar was the case in the ionization chamber when doping was in progress. The ionization chamber is a part of the permanent end-station of the I411 beamline at the Swedish National Synchrotron Radiation Facility MAX-lab. The ionizing radiation created by an undulator crossed the nanoparticle beam at 90°. The photon energy of 100 eV has been used to provide the optimal ionization cross-sections of the metals involved. The 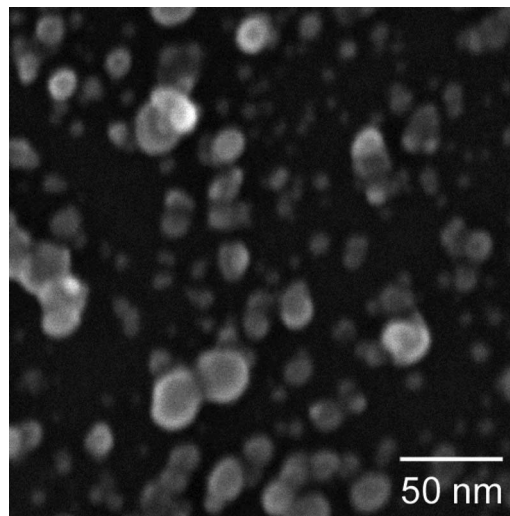photoelectrons were collected by a hemispherical electron energy analyzer (Scienta R4000). The binding energy spectra in the regions of both Yb 4f and Al 2p core levels were recorded. Since the nanoparticles were free, non-supported, the binding energy in the spectra was referenced relative to the vacuum level. All the spectra have been calibrated using the known Ar 3p lines of gaseous argon[20] present in the beam.

The size of the nanoparticles has been estimated after their deposition on a naturally oxidized Si(111) substrate and consequent *ex situ* scanning electron microscopy (SEM) imaging. As can be seen from Figure 1 the diameter of deposited nanoparticles is in the 5–10 nm range. The larger particles also seen in the image we attribute mostly to several agglomerated smaller ones – judging from the shapes of the former. Thus estimated dimensions are in a good agreement with the values earlier derived for our apparatus from the photoelectron spectroscopy studies on various metal nanoparticles. The PES-based method of size estimation relies on the so-called conducting sphere approximation which relates the difference in the electron binding energy between the macroscopic metal and the nanoparticles to the nanoparticle dimensions, see, for example, Ref. 21.

FIG. 1. Scanning electron microscopy (SEM) image of Yb-Al nanoparticles deposited on naturaly oxidized Si(111) substrate.

III. RESULTS AND DISCUSSION

A. Element distribution in free Yb-Al nanoalloy particles as seen by PES

It is the comparative analysis of photoelectron spectra which has allowed us disclosing the distribution of components in the bi-metallic nanoparticles. Figure 2(a) shows two typical Yb 4f spectra of nanoparticles created out of mixed Yb-Al vapor and out of pure Yb, the latter for reference. Both spectra have been recorded with the same instrumental resolution. In pure Yb nanoparticles the spectral responses of surface and bulk atoms with corresponding spin-orbit split $4f_{5/2}$ and $4f_{7/2}$ components are clearly resolved[16] and resemble those of supported Yb multilayers.[22] From Figure 2(a), one notices that the *highest* binding energy feature of the mixed Yb-Al case is at the same energy as the surface $4f_{5/2}$ feature
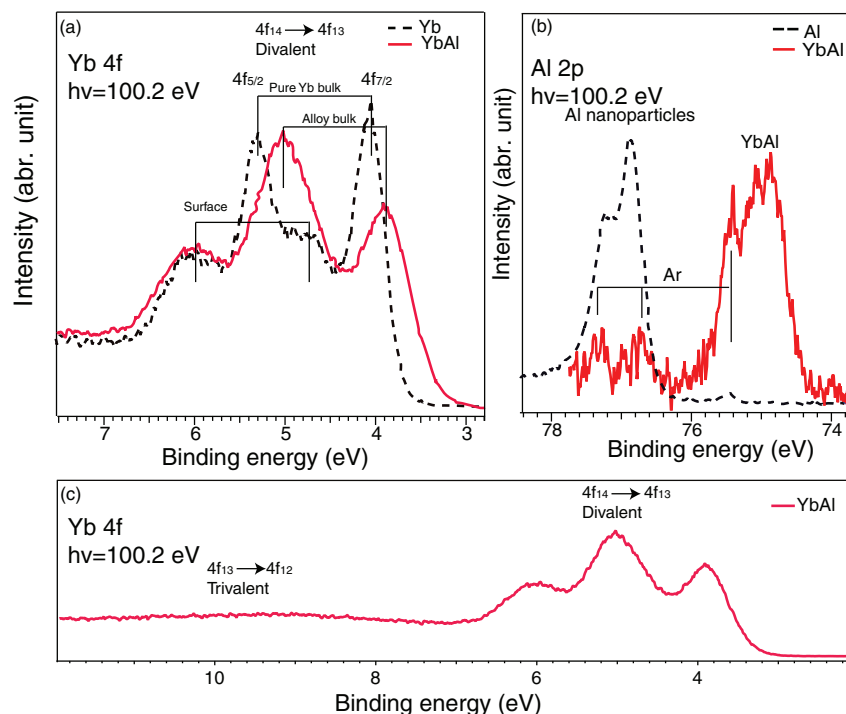
FIG. 2. (a) Photoelectron spectra recorded in Yb 4f region for pure Yb nanoparticles (dotted black line) and Yb-Al nanoalloy particles (solid red line) produced by our gas-aggregation source with magnetron sputtering. While the surface response is similar in both cases, the bulk response is different. (b) Photoelectron spectra recorded in Al 2p region for pure Al nanoparticles (solid dotted line) and Yb-Al nanoalloy particles (solid red line). (c) Photoelectron spectra of Yb-Al nanoalloy particles recorded in extended Yb 4f region where also the trivalent Yb appears in the case of well-mixed alloy. No corresponding features were observed there for our nanoparticles.

for pure Yb nanoparticles. Moreover, both features have similar width. In the view of this close similarity we assign the highest-energy feature of the mixed-case spectrum as due to the 4$f_{5/2}$ surface response of the nanoparticles formed out of Yb-Al vapor. The other, 4$f_{7/2}$ spin-orbit component of the surface response is obscured in the mixed Yb-Al case. This first analysis suggests that the nanoparticles formed out of Yb-Al vapour have their surface layer out of Yb. Such a conclusion is supported by the shape of the mixed-case spectrum as a whole. Indeed, visually, the pure-case spectrum has *four* well-resolved peaks, while the mixed-case spectrum has only *three*. Similar to the latter spectral shapes – with three instead of four peaks – have been reported in the PES studies of few ytterbium monolayers deposited on different metallic substrates. Nyholm *et al.*[23] observed such spectral shape after the deposition of a thin Yb layer on an Al monocrystal. Mårtensson *et al.* have found[24] that for two completed Yb monolayers on molybdenum surface the 4f spectrum also had three maxima and that the binding energy of Mo/Yb interface showed up as the lowest in energy out of three peaks – about 0.5 eV below pure Yb 4$f_{7/2}$ bulk.[24] Also in a later study of Yb layers grown on aluminum[25] three main peaks have been detected for two-monolayer coverage. Analogously to Yb on Mo, the lowest-energy peak was interpreted as due to the Yb-Al interface. Based on these spectroscopic results for deposited Yb on Al and Mo, we can suggest that the Yb-covered surface of our mixed-case nanoparticles surrounds a core out of the other metal, aluminum. Similarly to a deposited thin Yb layer,[23–25] the lowest-energy peak of the nanoparticle mixed-case spectrum in the Yb 4f region is due to the ytterbium atoms coor-

dinated to aluminum, i.e., the interface between Yb shell and Al core. The interface response is noticeably broader than the pure bulk feature, as expected for the more diverse Yb environment at the interface. As will be shown below, this hypothesis of a pure Yb surface surrounding a core containing mostly Al is supported by the Al 2p photoelectron spectrum of the nanoparticles.

In the present work the Al 2p feature is observed to shift significantly down (Figure 2(b)): by $\approx$2 eV compared to the pure Al nanoparticle response, earlier recorded by us.[26] In all mono-elemental nanoparticles produced by our source the core-level binding energy is within just 0.1–0.3 eV from the corresponding macroscopic metal energy.[26] The latter value $E_{solid}^{vacuum}(Al\ 2p)$ relative to the vacuum level is calculated by adding Al work-function W_{Al} ($\approx$4.3 eV for polycrystalline Al[27]) to the Al 2p core-level energy $E_{solid}(Al\ 2p)$ known relative to the Fermi edge:[26,28]

$$E_{solid}^{vacuum}(Al2p) = E_{solid}(Al2p) + W_{Al}. \quad (1)$$

In the Yb-Al nanoparticles the experimental Al 2p energy is $\approx$2 eV *lower* than the solid limit value E_{solid}^{vacuum}(Al 2p) defined by expression (1). This discrepancy can be rationalized if one recollects that such energy decrease is close to the difference in the work functions W_{Al} and W_{Yb} ($\approx$2.6 eV[29]) for Al and Yb elemental metals, respectively. If mostly Yb is on the surface of such nanoparticles then their work-function would be that of Yb, which is lower by almost 2 eV. If in expression (1) above one replaces W_{Al} by W_{Yb}, it indeed results in the corresponding lowering of the Al 2p energy relative to the vacuum

level: $E_{YbAl}^{vacuum} (Al\ 2p) = E_{Al} (Al\ 2p) + W_{Yb}$, as seen in our experiments.

An analogous situation has been observed by us for similarly produced NaK (sodium-potassium) nanoalloy particles, in which potassium dominated the surface layer.[17] Potassium on the surface reduced the vacuum-referenced Na $2p$ core-level energy of sodium present only in the core by the amount corresponding to the work-function difference between K and Na metals. As we argued in the NaK studies, in the self-assembling process it is energetically favorable to place the high cohesive-energy element – Na in the NaK alloy or Al in the Yb-Al alloy – into the nanoparticle core. Also the size of the atoms matters: Larger atoms, like potassium in NaK or ytterbium in Yb-Al are pushed to the surface of nanoparticles.[30]

In the Yb-Al case, the photoelectron spectra also provide information on the composition of the nanoparticle interior/"bulk," since the composition and the electronic structure are specifically interconnected in Yb. In the conventional Yb-Al alloy Yb is trivalent with the $[Xe]4f^{13}5d^16s^2$ ground electronic configuration. This is different to the configuration typical for the elemental Yb metal -$[Xe]4f^{14}6s^2$. In the metal the f electronic shell is fully filled (f^{14}), while in the Yb-Al alloy one of the f electrons is donated to the valence ($f^{13}5d^1$). In the photoelectron spectra the tri-valency manifests itself as a multiplet of narrow lines in the binding energy range higher than that of the divalent Yb.[23,25] If there were Yb atoms in the interior of our nanoparticles with the bulk-like coordination to Al they would likely disclose themselves in such peculiar spectral features in the corresponding energy range. Figure 2(c) presents an Yb-Al nanoparticle spectrum extended to include the region where the trivalent Yb would appear. As no noticeable Yb-related features are observed above the Yb $4f^{14}$ region (Figure 2(c)), we conclude that the nanoparticle core does not contain any significant amounts of Yb, but instead consists primarily of aluminum. Similar segregation has been observed by Nyholm *et al.*[23] for supported Yb-Al alloy layers.

Since in our case the interface peak in the Yb $4f$ spectrum of the nanoparticles is broad (Figure 2(a)), and since intensity is present where pure Yb bulk is usually detected, it is also possible that a layer or two of pure Yb exist between the Yb surface monolayer and the interface to the Al core. A similar spectral response has been observed when the third Yb layer was deposited on Mo substrate.[24]

We summarize that both Yb $4f$ and Al $2p$ spectra suggest a *core-shell* structure of nanoparticles created via aggregation of mixed Al-Yb vapor. The energy-minimum considerations support this conclusion. The overall spectral response is consistent with the surface of such particles consisting of a pair of monolayers of ytterbium. Different fractions of the metals in the primary vapor mixture could, in principle, lead to variations of the nanoalloy particle composition.

The knowledge of approximate dimensions and composition allows making certain judgments on the number of atoms for each element and thus the fractions of material quantities. As an example, we can consider a 10-nm diameter nanoparticle (the upper size limit) with 2 layers of Yb on top of Al core. Such a choice of the number of layers is suggested

by the closeness of the spectral responses of our nanoparticles and of two Yb layers deposited on metallic substrates.[24,25] Two layers of Yb are about 1 nm thick (crystal constant is ≈ 5.5 Å), what makes the Al core diameter to ≈ 8 nm. There can be different approaches for estimating the number of atoms in a metallic nanoparticle. One way is to use the solid density and assume spherical volume for the particle. Such an approach gives $\approx 1.6 \times 10^4$ aluminum atoms in the 8-nm diameter core. Calculating the number of Yb atoms in the shell is somewhat more ambiguous. If one divides the area of a spherical monolayer by the area occupied by a single atom the number of atoms in such a layer can be estimated. Such an approach gives for two Yb monolayers of the outer shell in question 1.3×10^3 and 1.0×10^3 atoms correspondingly. It makes the ratio of Al to Yb of about 7:1 in the number of atoms. Clearly, one has to take these numbers as giving only a very rough idea of the situation. At the same time it is worth making such estimates anyway for illustrating the capabilities of the method to extract quantitative, element-specific information from separate nanoparticles of complex composition.

B. Yb-Al nanoalloy particles–oxidized

As outlined in Sec. II, our second step has been the *in situ* oxidation of the Yb-Al particles by exposing the nanoparticle beam to a concentric radial oxygen flow. In our study on oxidation of pure Yb nanoparticles[16] we established that such doping did oxidize ytterbium surface. There, in the "ultimate" oxidation case the spectra appeared as two broad peaks separated by ≈ 1 eV, i.e., close to the characteristic for Yb $4f$ spin-orbit splitting. Each spin-orbit component of the oxide response has been centered at binding energy in between the corresponding *metallic*-nanoparticle surface and bulk. These spectra resembled to a large degree those known for the surface-oxidized macroscopic divalent ytterbium.[31] In contrast to the typical trivalent bulk oxide – with Yb_2O_3 composition, this rare-earth metal exhibits reduced valency at the surface, also in nanoparticles.

We have performed a series of measurements, in which the amount of O_2 used for doping was stepwise increased, and the spectra corresponding to each O_2 pressure were recorded. A typical series of spectra for different doping conditions is shown in Figure 3, with the oxygen amount increasing from zero in spectrum (a) (the same as Figure 2(c) for non-oxidized Yb-Al nanoparticles) to the maximum O_2 doping pressure in spectrum (e). Already at the lowest oxygen pressure involved, ≈ 1 mbar, changes in the Yb $4f$ spectra region are noticeable (spectrum (b)). The Yb-Al interface peak, observed in the non-oxidized case at the binding energy of about 4.0 eV, moves up by ≈ 0.2 eV in spectrum (b). We have earlier seen a similar upward binding energy shift of the bulk Yb $4f$ peak at intermediate oxidation conditions for pure Yb nanoparticles in our previous work on Yb.[16] There we have attributed it not to the changes in the bulk itself, but to the changes in the surface monolayer, which then became oxidized. Analogously, here for the Yb-Al alloy nanoparticles we attribute the upward shift of the interface peak to the same reason: to the appearance of Yb surface oxide coordinated to the interface layer of Yb.
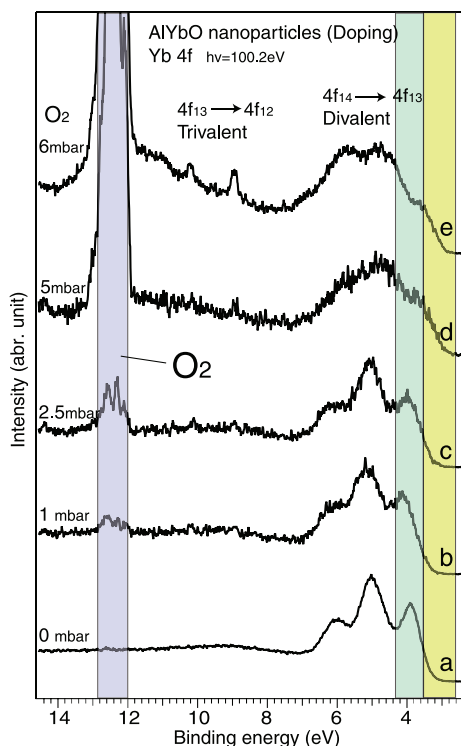
FIG. 3. (a)–(e) Photoelectron spectra of Yb-Al alloy nanoparticles oxidized by the "doping" method. From (a) to (e), the oxygen doping pressure increases. The gaseous O_2 region is shown by a vertical light blue stripe, and the Yb $4f_{7/2}$ interface region in non-oxidized nanoparticles is marked with a vertical light green stripe, while the alloy bulk oxide region at lower binding energy is marked with a light yellow band.

Judging from our earlier study of pure Yb nanoparticle oxidation, one should not expect a very strong change of the surface response at the intermediate oxidation conditions, and indeed this is the case also for Yb-covered alloy nanoparticles. The $4f_{5/2}$ surface response, which for the non-oxidized alloy does not overlap with the other features in the spectrum and has a well-defined maximum at ≈ 6 eV, is still well distinguished at about the same position but becomes broad, flat and without a clear maximum (Figures 3(b) and 3(c)). This shape bears a witness of more than one peak contributing to it. Only when the oxygen doping pressure is two times the value of case (c), ≈ 5 mbar, the changes in the spectrum become noticeable: all the features are nearly smeared out (Figure 3(d)). Though one can still trace three "peaks" in spectrum (d), their relative intensity becomes significantly different. The two peaks at ≈ 5 eV and at ≈ 4 eV, which are to a great extent due the Yb-Al interface $4f_{5/2}$ and $4f_{7/2}$ responses, loose in intensity relative to the surface response (at ≈ 6 eV). We attribute this to the covering of the nanoparticle surface by a completed layer of Yb oxide: the interface is poorly seen now since it became buried deeper in the bulk. The last spectrum (e) in Figure 3 is the case corresponding to the highest oxygen pressure. Here the shape of the spectrum becomes to a large extent the same as for pure YbO in the case of the "ultimate" oxidation by doping:[16] two peaks of close intensity and shape, separated by ≈ 1 eV. The interface $4f_{5/2}$ component (≈ 4 eV), however, seems to be still distinguishable in spectrum (e), though of relatively low intensity. A peculiar detail of the interface response is its shift

back toward lower binding energy – relative to the intermediate oxidized case (b). The interface response is now (spectrum (e)) even below its position in the non-oxidized case (a). An attempt to explain the nature of this shift may seem somewhat speculative since the chemical structure and the element coordination in the Yb-Al nanoparticles becomes rather complex. Nevertheless, we suggest a hypothesis based on the divalent oxide studies in Ref. 32. (We have used this hypothesis already in our interpretation of YbO spectra in Ref. 16.) In Ref. 32 it has been concluded that the signal of the oxidized bulk Yb appeared at lower energies than that of metallic bulk. In our Yb-Al case with high doping pressure, the interface layer can become oxidized, since oxygen can penetrate under the surface. In such a case the interface (which is a layer in the bulk) would respond at lower binding energy – judging from Ref. 32. Such a scenario seems feasible to assume, since Yb is known to let oxygen into the bulk of its crystal.[32]

Since we have not observed trivalent Yb oxide when pure ytterbium was oxidized in the earlier work, there have been no strong grounds to expect it in the present experiments where only a pair of Yb layers covered the surface of Al core. As mentioned above, trivalent Yb would appear as a set of narrow lines at the binding energies higher than the divalent $4f^{14}$ Yb response. In the "ultimate" oxidation case (e) of Figure 3, there is some intensity in this region –under and below molecular O_2 lines. This intensity, however, we attribute rather to the bound oxygen 2p-levels in the surface oxide. Indeed, this intensity is a continuum and not sharp well-defined lines.

In the Al 2p photoelectron spectra for the oxidized Yb-Al nanoparticles no significant change in the spectral position has been observed with the doping pressure increase. The intensity decreased noticeably, however. In Figure 4 we compare the cases without oxidation and with the strongest oxidation (corresponding to case (e) in Fig. 3). As can be seen from the figure, the discussed above downward shift of Al 2p binding energy (about 2 eV) is the same in both cases. The shape of the Al 2p spectrum is defined in general mainly by the interplay of the not-resolved bulk and surface components. In the oxidized case it seems to be more symmetric than in the metallic one. The bulk sub-component in the Al 2p response of nanoparticles is known to be at lower binding energy than the corresponding surface one.[26] Thus, it is tempting to assign some physical meaning to the disappearance of intensity on the lower energy side of Al 2p signal in the oxidized case when compared to the non-oxidized case (Figure 4). One possible explanation could be that the inner part of the nanoparticles, in this case the aluminum core, becomes buried even deeper when the oxide layer is formed on the surface. Due to that we do not see the inner part (the bulk) of the Al core.

The response of oxidized Al would appear in nanoparticles at ≈ 2 eV higher binding energy than that of its metallic core, as seen from third spectrum shown in Figure 4 – of pure Al nanoparticles, also created in our apparatus and oxidized using the doping method. This means that in the oxidized Yb-Al spectrum (Figure 4), we should have seen the Al oxide response, if any, at ≈ 77 eV binding energy. There seems to be some intensity in this region, but due to the weak response of Al (hidden in the bulk) a reliable judgment on whether the Al-oxide has been formed is difficult.
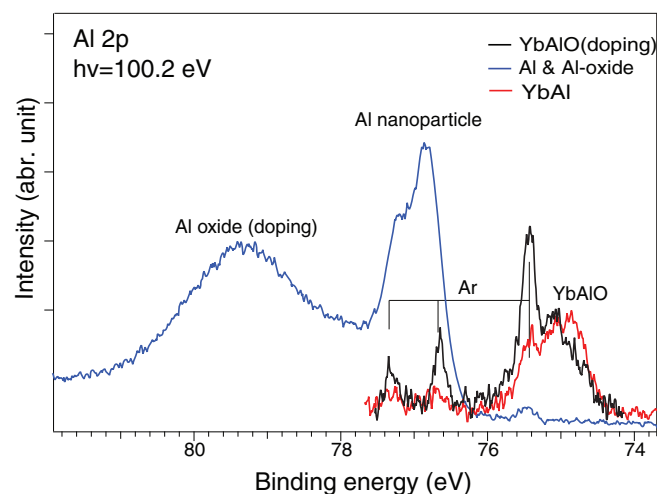
FIG. 4. Photoelectron spectra in Al 2*p* binding energy region: (1) of oxidized Yb-Al nanoparticles (solid black); (2) of non-oxidized Yb-Al nanoparticles (solid red); and (3) of pure Al nanoparticles containing Al-oxide (solid blue).

IV. CONCLUSIONS

In conclusion, we have produced nanoalloy bi-metallic Yb-Al particles using our in-house built vapor-aggregation-based apparatus with magnetron sputtering for creating primary vapor. Subsequently the particles have been oxidized using the "doping" technique. Having deposited the nanoparticles on a substrate we have been able to estimate their size range, using scanning electron microscopy images, to be from 5 to 10 nm. By *in situ* probing of the nanoparticles with photoelectron spectroscopy, their structure could be deduced. Aggregation of the mixed Yb-Al atomic vapor forms core-shell nanoalloy particles, with Yb atoms in the surface shell of few layers thickness, and Al atoms in the core. The surface segregation of Yb is consistent with kinetic and thermodynamic considerations: when the particles are being formed inside the cryostat there is enough atomic mobility for them to approach the lowest-energy configuration. Aluminum, which has higher cohesive energy (3.4 eV against 1.6 eV for Yb[33]) and which atoms are much smaller in size, is energetically considerably more favorable to place in the core. The reduction of the total energy of an atomic ensemble in the process of condensation from the vapor to the solid should be higher for a segregated final configuration, as has been experimentally observed by us for several bi-component nanoparticles produced by the same method (Yb/YbO,[16] NaK,[17] CuAg,[18] and Pb/PbO[19]). The exposure of segregated Yb-Al nanoalloy particles to molecular oxygen oxidizes at least the outer shell of Yb atoms. At intermediate oxidation conditions not all layers of Yb surface shell seem to be oxidized, but a "sandwich-like" structure of YbO/Yb/Al is likely to be the case. At the higher O_2 doping pressures also the deepest Yb layer at the interface to the aluminum core is very probably oxidized, leading to the Al-YbO core-shell structure. The results of the present study should be considered when photonics applications of Yb-doped garnet nanoparticles[13,15] are discussed.

[1]N. A. Mashayekhi, Y. Y. Wu, M. C. Kung, and H. H. Kung, Chem. Commun. **48**, 10096 (2012).
[2]Y. Sun and Y. Xia, Science **298**, 2176 (2002).
[3]C. Li, L. Yang, J. Xiao, Y.-C. Wu, M. Søndergaard, Y. Luo, D. Li, Q. Meng, and B. B. Iversen, Phys. Chem. Chem. Phys. **15**, 8710 (2013).
[4]A. A. Audi and P. M. A. Sherwood, Surf. Interface Anal. **33**, 274 (2002).
[5]N.-H. Cho, T.-C. Cheong, J. H. Min, J. H. Wu, S. J. Lee, D. Kim, J.-S. Yang, S. Kim, Y. K. Kim, and S.-Y. Seong, Nat. Nanotechnol. **6**, 675 (2011).
[6]R. F. Oulton, V. J. Sorger, T. Zentgraf, R.-M. Ma, C. Gladden, L. Dai, G. Bartal, and X. Zhang, Nature (London) **461**, 629 (2009).
[7]X. Yin, Z. Ye, J. Rho, Y. Wang, and X. Zhang, Science **339**, 1405 (2013).
[8]C. L. Nehl, H. Liao, and J. H. Hafner, Nano Lett. **6**, 683 (2006).
[9]W. Liu, A. E. Miroshnichenko, D. N. Neshev, and Y. S. Kivshar, ACS Nano **6**, 5489 (2012).
[10]N. Lopez, T. V. W. Janssens, B. S. Clausen, Y. Xu, M. Mavrikakis, T. Bligaard, and J. K. Nørskov, J. Catal. **223**, 232 (2004).
[11]D. Alloyeau, C. Ricolleau, C. Mottet, T. Oikawa, C. Langlois, Y. Le Bouar, N. Braidy, and A. Loiseau, Nat. Mater. **8**, 940 (2009).
[12]L. Lu, G. Burkey, I. Halaciuga, and D. V. Goia, J. Colloid Interface Sci. **392**, 90 (2013).
[13]S. Yoo, M. P. Kalita, A. J. Boyland, A. S. Webb, R. J. Standish, J. K. Sahu, M. C. Paul, S. Das, S. K. Bhadra, and M. Pal, Opt. Commun. **283**, 3423 (2010).
[14]Y. Ma, P. Zhou, R. Tao, L. Si, and Z. Liu, Opt. Lett. **38**, 1019 (2013).
[15]R. Su, P. Zhou, X. Wang, H. Zhang, and X. Xu, Opt. Lett. **37**, 3978 (2012).
[16]C. Zhang, T. Andersson, O. Björneholm, X. Xu, M. Tchaplyguine, and Z. Liu, J. Phys. Chem. C **117**, 14390 (2013).
[17]M. Tchaplyguine, S. Legendre, A. Rosso, I. Bradeanu, G. Öhrwall, S. Canton, T. Andersson, N. Mårtensson, S. Svensson, and O. Björneholm, Phys. Rev. B **80**, 033405 (2009).
[18]M. Tchaplyguine, T. Andersson, C. Zhang, and O. Björneholm, J. Chem. Phys. **138**, 104303 (2013).
[19]C. Zhang, T. Andersson, S. Svensson, O. Björneholm, and M. Tchaplyguine, Phys. Rev. B **87**, 035402 (2013).
[20]A. Kikas, S. J. Osborne, A. Ausmees, S. Svensson, O.-P. Sairanen, and S. Aksela, J. Electron Spectrosc. Relat. Phenom. **77**, 241 (1996).
[21]V. Senz, T. Fischer, P. Oelßner *et al.*, Phys. Rev. Lett. **102**, 138303 (2009).
[22]W.-D. Schneider, C. Laubschat, and B. Reihl, Phys. Rev. B **27**, 6538 (1983).
[23]R. Nyholm, I. Chorkendorff, and J. Schmidtmay, Surf. Sci. **143**, 177 (1984).
[24]N. Mårtensson, A. Stenborg, O. Björneholm, A. Nilsson, and J. Andersen, Phys. Rev. Lett. **60**, 1731 (1988).
[25]R. Fasel, P. Aebi, J. Osterwalder, and L. Schlapbach, Surf. Sci. **394**, 129 (1997).
[26]T. Andersson, C. Zhang, M. Tchaplyguine, S. Svensson, N. Mårtensson, and O. Björneholm, J. Chem. Phys. **136**, 204504 (2012).
[27]M. Uda, A. Nakamura, T. Yamamoto, and Y. Fujimoto, J. Electron Specrosc. Relat. Phenom. **88–91**, 643–648 (1998).
[28]P. H. Citrin, G. K. Wertheim, and Y. Baer, Phys. Rev. B **16**, 4256–4282 (1977)
[29]S. M. Sze, *Physics of Semiconductor Devices* (Wiley, New York, 1981).
[30]R. Ferrando, J. Jellinek, and R. L. Johnston, Chem. Rev. **108**, 845 (2008).
[31]Y. Takakuwa, S. Takahashi, S. Suzuki, S. Kono, T. Yokotsuka, T. Takahashi, and T. Sagawa, J. Phys. Soc. Jpn. **51**, 2045 (1982).
[32]R. Meier, E. Weschke, A. Bievetski, C. Schüßler-Langeheine, Z. Hu, and G. Kaindl, Chem. Phys. Lett. **292**, 507 (1998).
[33]C. Kittel, *Introduction to Solid State Physics*, 5th ed. (Wiley, New York, 1976).